Author(s): Xuejuan Zhang, Gongqiang You, Tianping Chen and Jianfeng Feng
Article Title: Maximum Likelihood Decoding of Neuronal Inputs from an Interspike Interval Distribution

Year of publication: 2009
Link to published version:
http://dx.doi.org/10.1162/neco.2009.06-08-807

Zhang, X. et al. (2009). Maximum Likelihood Decoding of Neuronal Inputs from an Interspike Interval Distribution. Neural Computation, Vol. 21, pp. 3079–3105

LETTER Communicated by Vincent Hakim

Maximum Likelihood Decoding of Neuronal Inputs from an Interspike Interval Distribution

Xuejuan Zhang
xuejuanzhang@gmail.com
Mathematical Department, Zhejiang Normal University, Jinhua, 321004, and Mathematical Department, Shaoxing University, Shaoxing, 312000, P.R.C.

Gongqiang You
ygq@163.com
Mathematical Department, Shaoxing University, Shaoxing, 312004, P.R.C.

Tianping Chen
tchen@fudan.edu.cn
Centre for Computational Systems Biology, Fudan University, Shanghai, 312000, P.R.C.

Jianfeng Feng
Jianfeng.Feng@warwick.ac.uk
Centre for Computational Systems Biology, Fudan University, Shanghai, 312000, P.R.C., and Department of Computer Science, Warwick University, Coventry CV4 7AL, U.K.

An expression for the probability distribution of the interspike interval of a leaky integrate-and-fire (LIF) model neuron is rigorously derived, based on recent theoretical developments in the theory of stochastic processes. This enables us to find for the first time a way of developing maximum likelihood estimates (MLE) of the input information (e.g., afferent rate and variance) for an LIF neuron from a set of recorded spike trains. Dynamic inputs to pools of LIF neurons both with and without interactions are efficiently and reliably decoded by applying the MLE, even within time windows as short as 25 msec.

1 Introduction

Neurons receive and emit spike trains, which are typically stochastic in nature due to the combination of their intrinsic channel fluctuations, the failure of their synaptic vesicle releases, and the variability in the input they receive. As a consequence, how to accurately and efficiently read out the input information from spike waves (simultaneously recorded multispike trains) remains elusive and is one of the central questions in (theoretical)

neuroscience (Rieke, Warland, & Steveninck, 1997; Gerstner & Kistler, 2002; Feng, 2003; Memmesheimer & Timme, 2006; Cateau & Reyes, 2006). For a given neuron or neuronal network, the most commonly used method to read out the input information is undoubtedly the maximum likelihood estimate (MLE), which is optimal under mild conditions. However, in order to rigorously perform the MLE, the prerequisite is knowing the exact expression of the interspike interval (ISI) distribution of efferent spikes of a neuron or a neuronal network. This is a difficult task in general. Even for the simplest leaky integrate-and-fire (LIF) model with constant input, such a distribution, which is equivalent to the first-passage of an Ornstein-Uhlenbeck (OU) process, was only obtained from the numerical inversion of its Laplace transform (Gerstner & Kistler, 2002; Tuckwell, 1988).

Other than in neuroscience, the first passage time of an OU process is also of prominent importance in many other fields, such as physics, engineering, and finance, and the topic has been widely addressed in many textbooks (Stratonovich, 1967; Risken & Frank, 1984; Gardiner, 1985). Thanks to recent developments (Göing-Jaeschke & Yor, 2003; Alili, Patie, & Pedersen, 2005) in stochastic process theory, three expressions of the interspike interval distribution have become available. The first two are deterministic methods based on the knowledge of Laplace transform of the first hitting time, and the third is a probability method in which the probability density of ISIs can be numerically simulated by the Monte Carlo method. Here we prefer to implement the third one, based on which the maximum likelihood estimate (MLE) for the LIF model is successfully developed. Despite the fact that the MLE for a spiking neural model has been discussed intensively by a few authors (Deneve, Latham, & Pouget, 1999; Sanger, 2003; Feng & Ding, 2004; Paninski, Pillow, & Simoncelli, 2004; Ditlevsen & Lansky, 2005; Truccolo & Eden, 2005), to the best of our knowledge, our approach is the first one based on the exact expression of the ISI distribution of the LIF model.

This letter presents an MLE strategy to decode statistic inputs (rate and variance) in a single LIF neuron. By calculating the related Fisher information as well as the confidence intervals of the model parameters, it is found that both the input rate and variance can be reliably decoded. We then employ the MLE to decode dynamic input signals for a spiking network. Within a short time window ($\sim$25 msec), the dynamic inputs can be read out accurately by an ensemble of 100 LIF neurons. This is an interesting result, and it may provide an answer to a puzzling issue in neuroscience. Thorpe, Fiz, and Marlot (1996) and Hung, Kreiman, Poggio, and DiCarlo (2005) pointed out that the required time from sensory inputs to motor reactions is around 200 msec. This suggests that only a few spikes can be generated in each layer to (encode) decode the input information and that the spikes should be deterministic rather than stochastic. Here we demonstrate that with neuron pools of a reasonable size, the input information can be read out reliably within a very short time window from random spikes if the

MLE is employed. Therefore, the stochasticity in spikes does not contradict the time constraint.

Certainly neurons in a microcolumn interact with each other. By including lateral inhibition and the time delay of the synaptic inputs, we find that the input information can still be reliably read out from spike waves of an interacting neuronal network using the MLE strategy mentioned above. The results should open up many new and challenging problems for further research in both theory and application. For example, we would ask how to implement MLE for multilayer interacting spiking neuronal networks.

2 Theoretical Results

2.1 Probability Distribution of ISIs of an LIF Neuron. We start our discussion from a single LIF model. When the membrane potential $V(t)$ is below the threshold V_{th}, its dynamics is determined by

$$dV = -\frac{V}{\gamma}dt + dI_{syn}(t),\ V \le V_{th}, \tag{2.1}$$

with $V(0) = V_{rest} < V_{th}$ and where γ is the decay time constant. The synaptic input is

$$I_{syn}(t) = a\sum_{i=1}^{m} E_i - b\sum_{j=1}^{n} I_j,$$

where $E_i = \{E_i(t), t \ge 0\}$, $I_j = \{I_j(t), t \ge 0\}$ are inhomogeneous Poisson processes with rates $\lambda_{E,i}$ and $\lambda_{I,j}$, respectively (Shadlen & Newsome, 1994), $a > 0$, $b > 0$ are the magnitudes of each excitatory postsynaptic potential (EPSP) and inhibitory postsynaptic potential (IPSP), and m and n are the total number of active excitatory and inhibitory synapses. Once $V(t)$ crosses V_{th} from below, a spike is generated, and V is reset to V_{rest}, the rest potential.

If there are numerous presynaptic inputs, we can use diffusion approximation to approximate the synaptic inputs (Tuckwell, 1988). For simplicity, we further assume $V_{rest} = 0, a = b, m = n$. Thus, the LIF model is simplified as

$$dV = -\frac{V}{\gamma}dt + \mu dt + \sqrt{\sigma}dB_t,\ V \le V_{th} \tag{2.2}$$

with

$$\begin{cases} \mu = a\lambda(t)(1-r) \\ \sigma = a^2\lambda(t)(1+r), \end{cases} \tag{2.3}$$

where $\lambda(t) = \sum_i \lambda_{E,i}(t)$ and $r\lambda(t) = \sum_j \lambda_{I,j}(t)$, r is the ratio between the inhibitory input and the excitatory input. If $\mu(t)\gamma = V_{th}$, the input is termed *exactly balanced input* because it ensures that the stable state of $V(t)$ is V_{th}, provided that noise is absent. Actually, the exactly balanced condition is equivalent to the following balanced relationship between λ and r:

$$r(t) = 1 - \frac{V_{th}}{a\lambda(t)\gamma}. \tag{2.4}$$

Biologically, equation 2.4 roughly describes the well-known push-pull effect of the inhibitory input to maintain the balanced inputs: the stronger the input (larger λ) is, the stronger the inhibitory input (larger r) is.

Feng and Ding (2004) derived an MLE formula of the input rate λ under the exactly balanced condition, equation 2.4. However, finding the exact MLE of the input for the general case remains an open question. In this letter, we develop an MLE strategy without this restriction, and both the input rate λ and the ratio r (or equivalently, σ) can be decoded at the same time. The idea of developing an MLE strategy of decoding both the input rate and the ratio between the inhibitory input and the excitatory input is interesting for biological applications (see section 4). One could easily adopt our approach to estimate other sets of parameters.

Let us first consider static inputs. The ISI of the efferent spikes can be expressed as

$$T = \inf\{t > 0 : V(t) \geq V_{th} | V(0) = 0\}, \tag{2.5}$$

which is a random variable. More precisely, we should define

$$\begin{cases} \tau_i = \inf\{t > \tau_{i-1} : V(t) \geq V_{th} | V(\tau_{i-1}) = 0\}, i \geq 1, \\ \tau_0 = 0, \end{cases} \tag{2.6}$$

and $T_i = \tau_i - \tau_{i-1}$, $i \geq 1$. It is readily seen that $\{T_i, i \geq 1\}$ is an independent and identically distributed (i.i.d.) sequence and has the identical probability density as T.

By setting $U = (V - \mu\gamma)/\sqrt{\sigma}$, the distribution of the ISIs of efferent spikes of the LIF model, equation 2.2, is equivalent to the distribution of the first-passage time of the following OU process,

$$dU = -\frac{U}{\gamma}dt + dB_t, \tag{2.7}$$

starting at $U_{re} = -\frac{\mu\gamma}{\sqrt{\sigma}}$ to hit $U_{th} = \frac{V_{th}-\mu\gamma}{\sqrt{\sigma}}$. The corresponding ISIs of efferent spikes can be expressed as

$$T = \inf\{t > 0 : U(t) \geq (V_{th} - \mu\gamma)/\sqrt{\sigma} | U(0) = -\mu\gamma/\sqrt{\sigma}\}. \tag{2.8}$$

Let $p_{\lambda,r}(t)$ be the probability density of T. As mentioned above, the first-passage time problem, which occurs in many areas, was once believed to have no general explicit analytical formula (Gerstner & Kistler, 2002), except a momentary expansion of the first-passage time distribution for constant input. Recently Alili et al. (2005) summarized what we know about the density of the first-passage time of an OU process, where three expressions of the distribution of T—the series representation, the integral representation, and the Bessel bridge representation—are presented. For numerical approximation, the authors pointed out that the first two approaches are easy to implement but require knowledge of the Laplace transform of the first hitting time, which can be computed only for some specific continuous Markov processes, while the Bessel bridge approach overcomes the problem of detecting the time at which the approximated process crosses the boundary (Alili et al., 2005). For this reason, we prefer to apply the Bessel bridge method under which the probability density of T has the following form (see the appendix),

$$\begin{aligned} p_{\lambda,r}(t) = &\exp\left(\frac{-V_{th}^2 + 2\mu\gamma V_{th}}{2\gamma\sigma} + \frac{t}{2\gamma}\right) p^{(0)}(t) \\ &\times E_{0\to V_{th}}\left\{\exp\left[-\frac{1}{2\gamma^2\sigma}\int_0^t (v_s - V_{th} + \mu\gamma)^2 ds\right]\right\}, \end{aligned} \tag{2.9}$$

where

$$p^{(0)}(t) = \frac{V_{th}}{\sqrt{2\pi\sigma t^3}} \exp\left(-\frac{V_{th}^2}{2t\sigma}\right) \tag{2.10}$$

is the probability density of the nonleaky integrate-and-fire model and $\{v_s\}_{0\leq s\leq t}$ is the so-called three-dimensional Bessel bridge from 0 to V_{th} over the interval $[0, t]$. Mathematically, it satisfies the following stochastic differential equation:

$$dv_s = \left(\frac{V_{th} - v_s}{t - s} + \frac{\sigma}{v_s}\right) ds + \sqrt{\sigma} dB_s, \quad 0 < s < t, \quad v_0 = 0, v_t = V_{th}. \tag{2.11}$$

In equation 2.9, $E_{0\to V_{th}}$ represents the expectation with respect to the stochastic process $\{v_s\}_{0\leq s\leq t}$ with starting point 0 and ending point V_{th}.

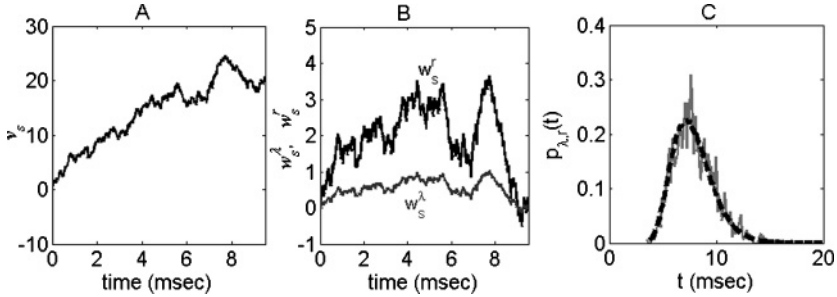

Figure 1: (A). Sampling trajectory of $\{v_s\}_{0\le s\le t}$ from 0 to $V_{th} = 20$. (B). Sampling trajectories of $\{w_s^\lambda\}_{0\le s\le t}$, $\{w_s^r\}_{0\le s\le t}$, which are the derivatives of $\{v_s\}_{0\le s\le t}$ with respect to λ and r, respectively. (C). $p_{\lambda,r}(t)$ (dashed curve) and histogram (solid curve) from a direct simulation of the LIF model.

At first glance, the expression of probability density 2.9 looks somewhat complicated, as it is an expectation of a singular stochastic process. However, we can use the Monte Carlo method to numerically evaluate the expectation. To do this, we have to generate a large number, say M, of independent sampling paths of a three-dimensional Bessel bridge. It should be pointed out that in numerical simulations, we do not use equation 2.11 to directly simulate the process $\{v_s\}_{0\le s\le t}$ since it is degenerate at $s = 0$. Instead we consider the process $\{v_s^2\}_{0\le s\le t}$, which satisfies

$$d(v_s)^2 = 2v_s dv_s + \sigma ds. \tag{2.12}$$

Note that the second term on the right-hand side of the equation above is due to the Ito integral. According to this, the iterating procedure to simulate the stochastic process v_s is as follows (we simply denote $v(j)$ as $v(j\Delta t)$):

$$\begin{cases} u(j+1) = u(j) + \Delta t \cdot \left(\dfrac{2v(j)(V_{th} - v(j))}{t - j\Delta t} + 3\sigma \right) \\ \qquad\qquad + 2v(j) \cdot \sqrt{\sigma} \cdot \Delta B(j), \\ v(j+1) = \sqrt{u(j+1)}, \end{cases}$$

with $v(1) = 0, u(1) = 0$ and where Δt is the time step. $\Delta B(j) = B(j\Delta t + \Delta t) - B(j\Delta t)$ is the increment of the Brownian motion with distribution *Norm* $(0, \Delta t)$. The three-dimensional Bessel bridge v_s has a trajectory as shown in Figure 1A.

Denote $\{v^i(k\Delta t)\}$ the ith sampling trajectory, and let

$$f_1(t) = \exp\left(\frac{-V_{th}^2 + 2\mu\gamma V_{th}}{2\gamma\sigma} + \frac{t}{2\gamma} \right) \cdot p^{(0)}(t).$$

Then the approximation formula for equation 2.9 is

$$\bar{p}_{\lambda,r}(t) = f_1(t) \cdot \frac{1}{M} \sum_{i=1}^{M} \exp\left[-\frac{1}{2\gamma^2\sigma} \sum_{k=1}^{n} (v^i(k\Delta t) - V_{th} + \mu\gamma)^2 \cdot \Delta t \right], \tag{2.13}$$

where $\Delta t = \frac{t}{n}$. The ISI density calculated from $p_{\lambda,r}(t)$ is plotted in Figure 1C, which demonstrates that $\bar{p}_{\lambda,r}$ matches the histogram obtained from a direct simulation of the LIF model very well.

2.2 MLE Decoding Strategy. Having an exact function of the distribution $p_{\lambda,r}(t)$, we can perform the MLE decoding procedure. The likelihood function is given by

$$L(\lambda, r) \stackrel{\Delta}{=} \prod_{i=1}^{N} p_{\lambda,r}(T_i), \tag{2.14}$$

where N is the total number of spikes. Then

$$\ln L(\lambda, r) = \sum_{i=1}^{N} \ln p_{\lambda,r}(T_i). \tag{2.15}$$

The optimal estimate of the input information (λ, r) corresponds to the root of the equation,

$$\begin{cases} \dfrac{\partial \ln L(\lambda, r)}{\partial \lambda} = 0 \\ \dfrac{\partial \ln L(\lambda, r)}{\partial r} = 0 \end{cases}. \tag{2.16}$$

Denote $w_s^x \stackrel{\Delta}{=} dv_s/dx$ $(x = \lambda, r)$. As the density function $p_{\lambda,r}(t)$ includes a singular stochastic process $\{v_s\}_{0\le s\le t}$ whose derivatives with respect to λ and r, that is, $\{w_s^\lambda\}_{0\le s\le t}$ and $\{w_s^r\}_{0\le s\le t}$, are also singular stochastic processes, we should pay additional attention to calculate $\partial \ln L/\partial x$ $(x = \lambda, r)$. First, let us derive the equation of w_s^x $(x = \lambda, r)$. It follows from equation 2.11 that w_s^x $(x = \lambda, r)$ satisfies the following equation,

$$dw_s = \left(\frac{-w_s^x}{t-s} + \frac{\sigma_x'}{v_s} - \frac{\sigma}{v_s^2} w_s^x \right) ds + \frac{\sigma_x'}{2\sqrt{\sigma}} dB_s, \quad x = \lambda, r, \tag{2.17}$$

where $\sigma_x' = \frac{\partial\sigma}{\partial x}$, $v_0 = 0$ and $w_0^x = 0$ $(x = \lambda, r)$. Sampling trajectories of w_s^λ and w_s^r are shown in Figure 1B.

Let

$$f_2(t) = \exp\left[-\frac{1}{2\gamma^2\sigma}\int_0^t (v_s - V_{th} + \mu\gamma)^2 ds\right];$$

then

$$\ln p_{\lambda,r}(t) = \ln f_1(t) + \ln E_{0\to V_{th}}[f_2(t)].$$

The derivatives of $f_1(t)$ and $f_2(t)$ are

$$\frac{\partial}{\partial x}\ln f_1(t) = h_x + \frac{V_{th}^2\sigma_x'}{2\sigma^2 t},$$

with

$$h_x = \frac{V_{th}^2\sigma_x'}{2\sigma^2\gamma} + \frac{(\mu_x'\sigma - \mu\sigma_x')V_{th}}{2\sigma^2} - \frac{\sigma_x'}{2\sigma},$$

and

$$\begin{aligned} g_x(t) &\triangleq \frac{\partial}{\partial x} f_2(t) \\ &= f_2(t)\cdot\frac{\sigma_x'}{2\sigma^2\gamma^2}\int_0^t \Bigg[(v_s - V_{th} + \mu\gamma)^2 - \frac{2\sigma}{\sigma_x'}(v_s - V_{th} + \mu\gamma) \\ &\quad \cdot (w_s^x + \mu_x'\gamma)\Bigg] ds, \quad x = \lambda, r. \end{aligned} \tag{2.18}$$

Then

$$\frac{\partial}{\partial x}\ln E_{0\to V_{th}}[f_2(t)] = \frac{E_{0\to V_{th}}\left[\frac{\partial}{\partial x} f_2(t)\right]}{E_{0\to V_{th}}[f_2(t)]} = \frac{E_{0\to V_{th}}[g_x(t)]}{E_{0\to V_{th}}[f_2(t)]}.$$

Therefore,

$$\frac{\partial \ln L}{\partial x} = N\cdot h_x + \frac{V_{th}^2\sigma_x'}{2\sigma^2}\sum_{i=1}^N T_i^{-1} + \frac{\sigma_x'}{2\sigma^2\gamma^2}\sum_{i=1}^N \frac{E_{0\to V_{th}}[g_x(T_i)]}{E_{0\to V_{th}}[f_2(T_i)]}, \quad x = \lambda, r. \tag{2.19}$$

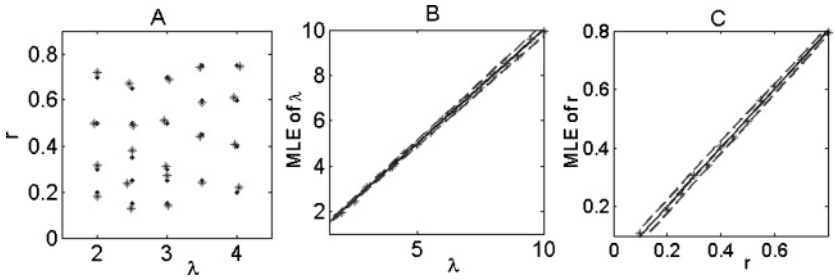

Figure 2: MLE of a single neuron. (A). MLE of (λ, r) from 1000 interspike intervals. Dots represent true values, while stars are estimated from the MLE method. (B). MLE (star points) of λ versus the input rate λ for a fixed ratio $r = 0.25$. (C). MLE (star points) of r versus the input rate r for a fixed input rate $\lambda = 7$. Parameters are $V_{th} = 20$ mV, $\gamma = 20$ msec, and $a = 2$.

Substituting equation 2.16 with 2.19, we know that the MLE of the input information (λ, r) is the root to the following two equations:

$$N \cdot h_\lambda + \frac{V_{th}^2 \sigma'_\lambda}{2\sigma^2} \sum_{i=1}^{N} T_i^{-1} + \frac{\sigma'_\lambda}{2\sigma^2\gamma^2} \sum_{i=1}^{N} \frac{E_{0\to V_{th}}[g_\lambda(T_i)]}{E_{0\to V_{th}}[f_2(T_i)]} = 0, \tag{2.20}$$

$$N \cdot h_r + \frac{V_{th}^2 \sigma'_r}{2\sigma^2} \sum_{i=1}^{N} T_i^{-1} + \frac{\sigma'_r}{2\sigma^2\gamma^2} \sum_{i=1}^{N} \frac{E_{0\to V_{th}}[g_r(T_i)]}{E_{0\to V_{th}}[f_2(T_i)]} = 0. \tag{2.21}$$

Though it is difficult to find an analytical solution to equations 2.20 and 2.21, we can numerically find its root, denoting it as $(\hat{\lambda}, \hat{r})$. Figure 2A depicts the value $(\hat{\lambda}, \hat{r})$ versus its actual value $(\lambda.r)$ for the model defined by equation 2.2, where each point of $(\hat{\lambda}, \hat{r})$ is obtained by using 1000 interspike intervals. It is clearly shown that the estimated value $(\hat{\lambda}, \hat{r})$ almost exactly matches the true value $(\lambda.r)$.

2.3 Fisher Information Matrix and Confidence Interval. Knowing the likelihood function, the information contents about the model parameters can be analyzed using another important statistical quantity, Fisher information, which sets the lowest bound of an unbiased estimate via Cramér-Rao inequality. Furthermore, when the sampling size is large enough, the central limit theorem tells us that the likelihood function asymptotically obeys a gaussian distribution whose mean is the true value of the parameter and whose covariance is the inverse of Fisher information matrix (Feng, 2003). Thus, the Fisher information also gives the confidence interval of the MLE.

Let us look at the Fisher information in our model. Define

$$\mathbf{I}_1(\lambda, r) = \begin{bmatrix} E\left(\frac{\partial \ln p_{\lambda,r}(t)}{\partial \lambda}\right)^2 & E\left(\frac{\partial \ln p_{\lambda,r}(t)}{\partial \lambda}\frac{\partial \ln p_{\lambda,r}(t)}{\partial r}\right) \\ E\left(\frac{\partial \ln p_{\lambda,r}(t)}{\partial \lambda}\frac{\partial \ln p_{\lambda,r}(t)}{\partial r}\right) & E\left(\frac{\partial \ln p_{\lambda,r}(t)}{\partial r}\right)^2 \end{bmatrix}. \tag{2.22}$$

As

$$\frac{\partial \ln p_{\lambda,r}(t)}{\partial x} = h_x + \frac{V_{th}^2 \sigma_x'}{2\sigma^2 t} + \frac{\sigma_x'}{2\sigma^2\gamma^2}\frac{E_{0\to V_{th}}[g_x(t)]}{E_{0\to V_{th}}[f_2(t)]}, \quad x = \lambda, r,$$

we can numerically calculate the four terms in the above matrix—for example,

$$\mathbf{I}_1(\lambda, r)_{11} = \int \left(h_\lambda + \frac{V_{th}^2 \sigma_\lambda'}{2\sigma^2 t} + \frac{E_{0\to V_{th}}[g_\lambda(t)]}{E_{0\to V_{th}}[f_2(t)]}\right)^2 p_{\lambda,r}(t)dt,$$

$$\mathbf{I}_1(\lambda, r)_{12} = \int \left(h_\lambda + \frac{V_{th}^2 \sigma_\lambda'}{2\sigma^2 t} + \frac{\sigma_\lambda'}{2\sigma^2\gamma^2}\frac{E_{0\to V_{th}}[g_\lambda(t)]}{E_{0\to V_{th}}[f_2(t)]}\right) \times \left(h_r + \frac{V_{th}^2 \sigma_r'}{2\sigma^2 t} + \frac{\sigma_r'}{2\sigma^2\gamma^2}\frac{E_{0\to V_{th}}[g_r(t)]}{E_{0\to V_{th}}[f_2(t)]}\right) p_{\lambda,r}(t)dt.$$

We also calculate the other two elements.

The Fisher information matrix is defined as

$$\mathbf{I}(\lambda, r) = N\mathbf{I}_1(\lambda, r).$$

For a given sampling number N, we have

$$(\hat{\lambda}, \hat{r}) \to Norm((\lambda, r), \mathbf{I}(\lambda, r)^{-1}),$$

in the distribution sense, or briefly,

$$(\hat{\lambda}, \hat{r}) \approx Norm((\lambda, r), \mathbf{I}(\lambda, r)^{-1}).$$

The confidence intervals of the model parameters $(\hat{\lambda}, \hat{r})$ for a given N can be computed as

$$\left[\lambda - \sqrt{(\mathbf{I}(\lambda, r)^{-1})_{11}}, \lambda + \sqrt{(\mathbf{I}(\lambda, r)^{-1})_{11}}\right],$$

$$\left[r - \sqrt{(\mathbf{I}(\lambda, r)^{-1})_{22}}, r + \sqrt{(\mathbf{I}(\lambda, r)^{-1})_{22}}\right],$$

where $(\mathbf{I}(\lambda, r)^{-1})_{ii}$ is the iith component of the inverse Fisher information matrix.

In Figures 2B and 2C, we plot the confidence intervals for parameters λ and r for $N = 1000$, respectively. Interestingly, one can see that the confidence interval of the parameter λ is enlarged, while the confidence interval of the ratio parameter r becomes smaller with the increase of input frequency. As Feng and Ding (2004), pointed out, the higher the input rate, the more variable the output spikes (i.e., the larger the CV, the smaller the Fisher information). This is why we observe such opposite increasing properties of the confidence intervals by noticing that increasing the ratio between the inhibitory input and the excitatory input tends to decrease the CV of the firing.

Remark. In our toy model here, we assume that the input takes the form of a Poisson process. Hence, the remaining variable in the input variance could be the ratio r or the EPSP magnitude. It is easily seen that our approach is equivalent to estimating the input mean and variance, although we estimate λ, r here. Certainly in many cases, the ratio r is fixed in a biological circuit. Suppose that only the input rate λ is to be decoded. The MLE of λ is the root to equation 2.20. The corresponding Fisher information is then given by

$$I(\lambda) = E\left(\frac{\partial \ln p_\lambda(t)}{\partial \lambda}\right)^2 = \int \left(h_\lambda + \frac{V_{th}^2 \sigma_\lambda'}{2\sigma^2 t} + \frac{E_{0\to V_{th}}[g_\lambda(t)]}{E_{0\to V_{th}}[f_2(t)]}\right)^2 p_\lambda(t)dt, \tag{2.23}$$

where $p_\lambda(t)$ has the same expression as equation 2.9 but with r being fixed. Thus, to estimate the single parameter λ, the confidence interval is

$$\left[\lambda - \frac{1}{\sqrt{NI(\lambda)}}, \lambda + \frac{1}{\sqrt{NI(\lambda)}}\right]. \tag{2.24}$$

2.4 Comparison with Rate Decoding. One might ask why we do not decode the input information by simply fitting the firing rate and CV since the first and second moments of ISIs are known. Such a rate decoding approach has been extensively discussed in the literature. It is known that when the sampling number is large enough, both MLE and rate coding methods give reasonable results. However, from the viewpoint of parameter estimation, the advantage of the MLE method is obvious. By the Cramér-Rao lower bound, we know that MLE is optimal but rate decoding is not.

To give a numerical comparison of the two approaches, let us fix the ratio $r = 0$ and perform decoding of the afferent rate λ. Figure 3A shows the MLE method and Figure 3B the rate decoding approach. It is known from equation 2.3 that with the input rate increasing, the variation also increases; thus, the errors of decoding with both the MLE and rate coding increase in the regime of high λ. However, as can be seen from Figure 3A,

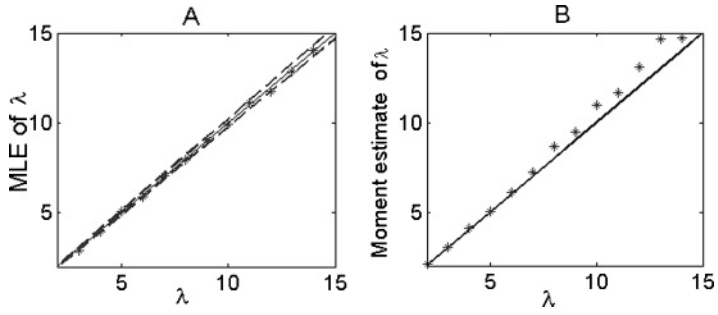

Figure 3: Comparison of two methods. (A) Estimate of afferent input λ via the MLE method. Dashed lines are confidence intervals calculated from equation 2.24. (B). Estimate of afferent input λ via the rate coding method. Here we fix $r = 0, a = 1$ and choose 200 ISI intervals.

the decoding error using the MLE method is bounded by the Cramér-Rao lower bound, while the error using the rate coding approach may be out of this range. From this point of view, the MLE is optimal. The advantage of the MLE over rate coding is quite obvious even for a relatively small sampling number (here we take $N = 200$).

3 MLE of Dynamic Inputs

3.1 Decoding of Dynamic Inputs in Networks Without Interactions. Usually a postsynaptic neuron receives dynamic inputs from presynaptic neurons, and we have to decode the input within a short time window. Based on the above decoding strategy, let us now further employ the MLE to decode dynamic inputs in pools of neurons. The network is composed of 100 neurons, as schematically plotted in Figure 4A. We assume that the input is varying slowly compared with the timescale of the neuronal dynamics, so that in each time window of fixed length T_W, the ISI distribution adiabatically follows the stationary one.

Under the exactly balanced condition, equation 2.4, the problem has been investigated by Rossoni and Feng (2007). However, the method presented there cannot be extended to a more general case without knowing the exact relationship between the input and the output of the LIF neuron. Nevertheless, on the basis of this theoretical development, we can now relax the restriction of the exactly balanced condition and read out both the input rate and variance from spike waves in a short time window (see Figure 4B).

To express the main idea of how to apply the MLE to decode dynamics input information, we assume that each neuron receives a common excitatory Poisson synaptic input ($r = 0$); the procedure below is also valid for

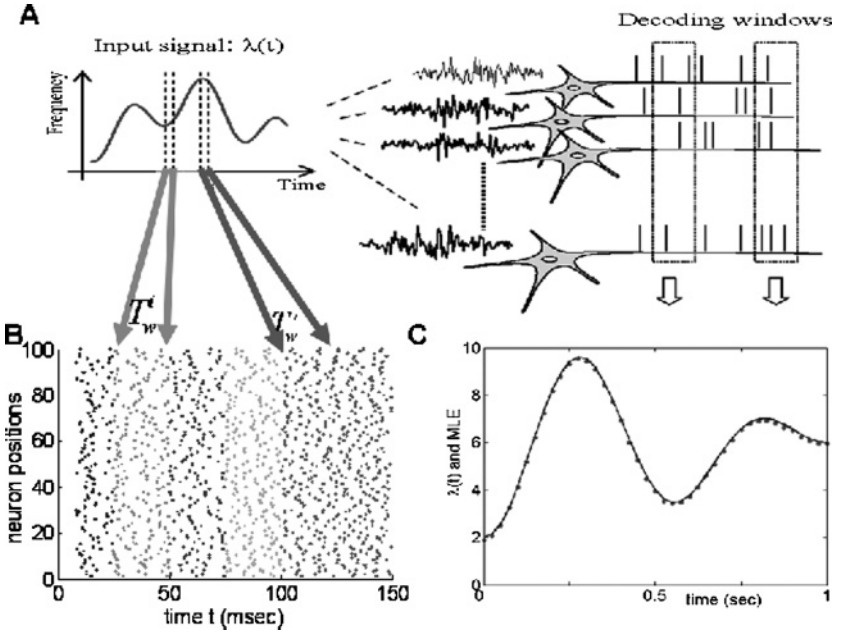

Figure 4: MLE in a network without interactions. (A) Schematic plot of reading dynamic inputs from an ensemble of neurons. For a fixed time window (indicated by T_w^i, T_w^j), the spikes are collected and the input is decoded by means of MLE. (B) Raster plot of spikes in five different decoding windows. The information is read out from the spikes in each window. (C) An example of reading out the dynamic input rates from an ensemble of neurons. The original signal $\lambda(t)$ is plotted in the continuous line, while dots are estimated values of $\lambda(t)$.

other ratios between the inhibitory input and the excitatory input. We suppose that the waveform of input is $\lambda(t) = 2 + 4(\sin^2(2\pi t) + \sin^2(\frac{3}{2}\pi t))$. Here the timescale of the input is measured in seconds; thus, it varies slowly compared with the timescale of the neuronal dynamics. Note that during the decoding procedure, any ISI longer than T_w will not be included in the MLE estimate, so the estimated input $\hat{\lambda}(t)$ is bound to be biased—a typical situation in survival analysis. To obtain an unbiased estimate, the censored intervals have to be included, and more detailed calculations are required. However, the numerical results (see Figure 4C) indicate that the bias is very limited, and we simply ignore the issue of censored intervals here.

Figure 4C depicts the MLE versus the input frequency for time windows $T_w = 25$ ms. Although T_w is very short, we can see that the estimate is excellent (except that it is slightly downward biased).

The results also provide a possible answer for a long-standing issue in neuroscience. Thorpe et al. (1996) pointed out that the time interval between

sensory inputs and motor outputs is around 200 msec. They then argued that only a few interspike intervals could be used to estimate the input in each layer, and therefore a stochastic dynamics is implausible in the nervous system. Our results clearly show that within a very short time window (∼25 msec), the spikes generated from an array of neurons contain enough information for the central nervous system to decode the input information. Hence, even without the overlap of the processing time of each layer in the nervous system, within 200 msec it could reliably read out the information for around 10 layers.

3.2 Decoding of Input Information in Networks with Interactions. So far we have assumed that neurons in the same column are regraded as independent. Certainly neurons in a microcolumn interact with each other, which might considerably change all conclusions in the previous sections. Can we or the central nervous system read out the input information from spike waves? In this section, we further investigate such an issue. The purpose is to read out the information of an external stimulus even in the presence of interactions between neurons in a microcolumn.

The strategy adopted here (or possibly by the nervous system) is based on including the lateral inhibition and the time delay of the synaptic inputs. As a result, all neurons in a network behave independently before the interactions kick in. The depolarization caused by the external inputs evokes the hyperpolarizing effect of inhibitory interactions between neurons, which subsequently shuts down the firing of all neurons (first epoch) and enables the neurons in the microcolumn to act independently again.

The model we consider here consists of $P_E = 100$ excitatory and $P_I = 100$ inhibitory neurons with all-to-all connectivity. The corresponding LIF equation for each neuron is

$$\frac{dV_j}{dt} = -\frac{V_j}{\gamma} + I_j^E(t) + I_j^S(t), \quad V_j \le V_{th}, \quad j = 1, 2, \ldots, N_n = P_E + P_I, \tag{3.1}$$

where

$$\begin{cases} I_j^E(t) = a\lambda_j(t) + a\sqrt{\lambda_j(t)}\xi_j(t), \\ I_j^S(t) = \displaystyle\sum_{k=1}^{P_E} \sum_{t_k^m+\tau<t} w_{jk}^E \delta(t - t_k^m - \tau) - r_{EI} \sum_{l=1}^{P_I} \sum_{t_l^m+\tau<t} w_{jl}^I \delta(t - t_l^m - \tau). \end{cases} \tag{3.2}$$

In the equation, $I_j^E(t)$ is the external input from the stimulus with an input rate $\lambda_j(t)$ and magnitude a, $\xi_j(t)$, and $j = 1, \ldots, N_n$ are independent white noises. $I_j^S(t)$ is the spiking input from other neurons to the jth neuron. $w_{jk}^E, k = 1, \ldots, P_E$ and $w_{jl}^I, l = 1, \ldots, P_I$ are EPSP and IPSP sizes that the

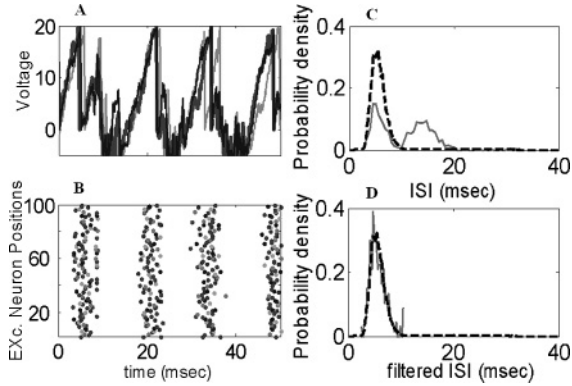

Figure 5: (A) Trajectories of three excitatory neurons in an interacting network for $\lambda = 4$, $D = 2$. (B) Raster plots of 100 excitatory neurons. (C) The histogram (solid curve) obtained from a direct simulation of the model and the theoretical density (dashed curve). (D) The solid curve is the histogram from the filtered interspike intervals (the first modes in C); the dashed one is the same as in B.

jth neuron receives from the kth and the lth neurons, r_{EI} is the ratio between the inhibitory and the excitatory interactions, t_k^m is the mth spike generated from the kth neuron, and τ is the synaptic time delay. We suppose that w_{jk}^E and w_{jl}^I are uniformly distributed in $[0, D]$ (D is termed the maximal coupling strength or, simply, the coupling strength), and $\lambda_i(t) = \lambda_j(t) = \lambda(t)$. In our numerical simulations, we fix $a = 1$, $\tau = 5$ msec, $r_{EI} = 1.8$.

Figures 5A and 5B show one simulation with the setup as above by fixing $D = 2$. As expected, with the application of the external inputs, all neurons start responding, and some fire a few spikes. However, once the inhibitory neurons fire, they send spikes to other neurons, which causes a hyperpolarization effect on these postsynaptic neurons, and all neuronal activities are shut down after a certain time delay of the synaptic transmission. Once the network becomes silent, the interactions between neurons disappear, and neurons in the network act as independent units again. Hence the external inputs evoke the second epoch of the spikes. This procedure repeats itself. Consequently, the network will produce rhythmic oscillations by properly cooperating the local inhibition and the time delay of the synaptic transmission, a well-known phenomenon observed in many biological experiments. In noisy networks of LIF neurons, it is shown that the oscillation frequency is of the order of the inverse of the synaptic delay (Brunel & Hakim, 2008). Here we will investigate how the network rhythm is related to information decoding.

We might ask ourselves why neurons use pulsed interactions to communicate between them rather than other forms of interactions such as gap junctions. The difference between gap junctions and pulsed interactions is

that the former exchange information continuously, while the latter only react to each other when the membrane potential exceeds a threshold that results in the independent phases in Figure 5B.

Based on such an inhibition-induced shutting-down mechanism, let us now investigate how afferent input rate $\lambda(t)$ can be read out accurately by applying the MLE strategy. The problem of introducing interactions in a fixed time window is that the decoding may have a significant bias. To resolve this issue, we first look at the histogram of the ISIs of equation 2.3 in the case that the input rate $\lambda(t)$ is time independent, say, $\lambda(t) = \lambda = 4$. It is clearly indicated in Figure 5C that the histogram now has two modes: the one with short ISIs corresponds to the actual ISIs driven by the external input, and the other is due to the interactions. After filtering out the second mode, the obtained histogram fits well with the theoretical density (the dashed trace in Figure 5D). To decode the input information, we filter out the spikes corresponding to the second mode and exclusively use the ISIs of the first mode. We will show that in a short time window, the input rate can be reliably decoded.

In Figures 6A and B, we test our algorithm in a dynamic input with waveform $\lambda(t) = 2 + 4(\sin^2(2\pi t) + \sin^2(\frac{3}{2}\pi t))$, for different values of coupling strength. Here t is measured in seconds, which ensures the ISI distribution being adiabatically stationary in each time window of length around 25 msec. To show the network behaviors under different coupling intensities, the ensemble voltage traces and the corresponding raster plots of 100 excitatory cells for $\lambda(t) = \lambda = 3$ are depicted in the top and middle panels of Figures 6A and 6B, respectively. Interestingly, the network displays rhythmic activity when the coupling strength is strong and the decoding (shown in the bottom trace of Figure 6B) is quite accurate; however, for weak values of the coupling strength, no rhythmic activities are observed, and, as expected, the estimated values (see the bottom trace of Figure 6A) are much less accurate than in the rhythmic case.

Figures 6A and 6B suggest that there should exist a critical value of the coupling strength D_c, after which the network can perform decoding accurately. To see this, we plot the relative decoding error $\frac{\hat{\lambda}-\lambda}{\lambda}$ versus the coupling intensity D in Figure 6C, for constant afferent inputs (we choose $\lambda = 4$, $\lambda = 5$, and $\lambda = 8$). For $D = 0$, the decoding is very accurate, which is the case discussed in section 3.1. When D slightly increases, the absolute decoding error increases. This is because the interactions between neurons cannot be shut down for weak coupling strengths. After about $D = 0.25$, the absolute decoding error gradually decreases, and after about $D = 0.8$, the input rate can be reliably read out; meanwhile, the network exhibits clear rhythmic activities.

If only interspike intervals are concerned, then for a time window that is too short, it is difficult to perform a decoding task because there are not enough spikes. And if the time window is too long, the informative interspike intervals generated by the external inputs interfere with the ones

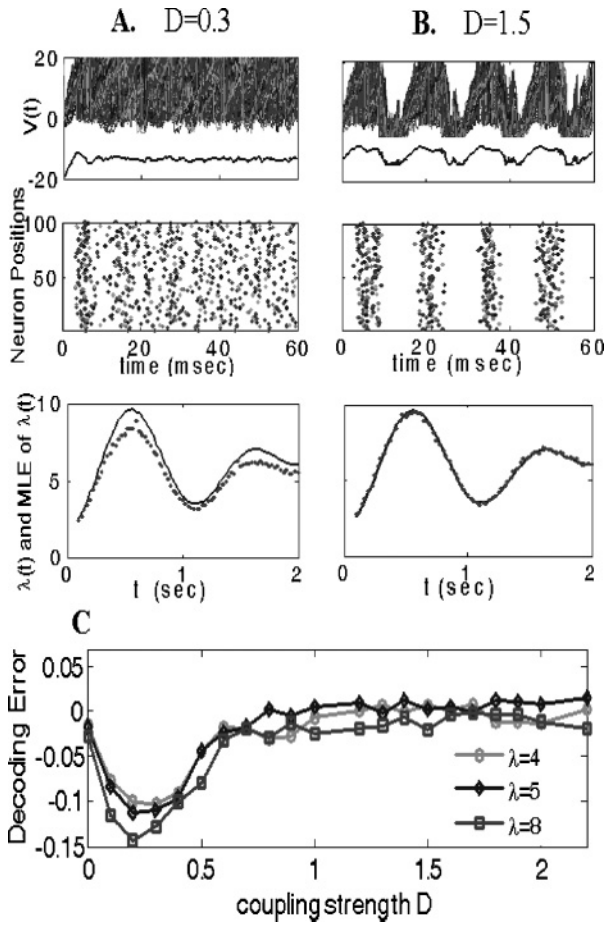

Figure 6: MLE in a network with interactions. (A, B) Top traces: The trajectories of 100 excitatory neurons and the corresponding mean voltages for $\lambda = 3$ during $0 \sim 60$ ms. Middle traces: Raster plots corresponding to the above trace. Bottom traces: Reading out the dynamic inputs (the solid curve) from 100 excitatory neurons, every dot is estimated by the MLE approach within a fixed time window of $T_w = 25$ msec. Left column is for $D = 0.3$, and right column is for $D = 1.5$. (C) The optimal coupling intensities for reading out the input information within a fixed time window $T_w = 25$ msec.

due to interactions. We conclude that there should be an optimal decoding time window T_w^{optim} in which the input information is optimally decoded. To test this, we plot the relative decoding errors $\frac{|\hat{\lambda}-\lambda|}{\lambda}$ versus different time windows for intermediate input rates in Figure 7A and for high input rates in Figure 7B. It is shown that for moderate input rates ($2 \leq \lambda \leq 5$), such

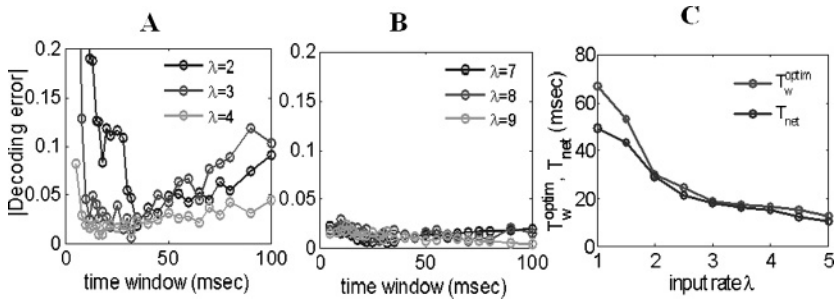

Figure 7: (A) Decoding errors of reading out intermediate input rates within different time windows, where optimal time windows are shown to be around 15 to 40 msec. (B) Decoding errors of reading out high input rates are shown to be very small within both short and large time windows. (C) Relationship of the optimal decoding windows and the periods of the network oscillations. For moderate input rates, $T_w^{optim} \approx T_{net}$. $D = 1.5$.

optimal windows exist and are around 15 to 40 msec, which are in the gamma range; for a high input rate λ, the decoding errors are small (<5%) for both the short and long time windows. The accuracy of decoding with high input rates stems from the fact that spikes are generated within a very short time (5 msec or less, the synaptic delay time), which implies that neurons in a pool have no time to interact with each other before starting the next epoch of firings. Hence, in response to a high input rate, neurons in a network act independently. This is why a small decoding error is achieved even for long time windows.

To explore how the optimal decoding windows for moderate input rates come about and how they are related with the periods T_{net} of the network oscillations, we further depict these two time windows (T_{net} and T_w^{optim}) versus the input rate λ in Figure 7C. The definition of T_{net} is clear (see Figure 6B). For a reasonable range of input rates λ (about $2 \leq \lambda \leq 5$), the optimal decoding windows are approximately equal to the network periods. The consistency of the optimal decoding windows and the periods of the network oscillations for moderate input rates shows that the spikes generated from a pool of neurons within the period of the network rhythm are sufficient to read out input rates. Time windows that are too small or too large will either have insufficient input information or redundant interspike intervals, both of which will introduce bias in decoding. The results in Figures 6 and 7 may serve as a good example to show the functional role of the gamma rhythm (30 to 80 Hz) in information processing, which has been extensively discussed by many authors (see Buzsáki, 2006).

3.3 Tracking a Moving Stimulus. Now let us consider a more biologically realistic setup. Assume that an ensemble of identical but independent

neurons, say 1000 LIF neurons, are grouped into $N = 10$ columns, and each 100 neurons in a same column share an identical tuning curve defined by

$$\lambda(x_i; x(t)) = \lambda_0 + c \cdot \lambda_0 \exp\left(-\frac{(x(t) - x_i)^2}{2d^2}\right), \tag{3.3}$$

where c is a constant scaling factor, d is the tuning width, x_i is the column's field center, and x is the position. For example, the neuron in the ith column receives an input that is the position information $x(t) \in [0, L]$ (we take $L = 11$ here), and the response of the neuron is given by $\lambda(x_i, x(t))$. The task is to read out the position information $x(t)$. The setup mimics the situation of reading out the position of a rat from simultaneous recordings of place cells in hippocampus (Truccolo & Eden, 2005).

For simulation, we fix $c = 2$, $d = 1.5$, and $\lambda_0 = 2$. We assume that the target position x changes in time according to $x(t) = \sum_{j=1}^{N} \xi_j \chi(t \in I_j)$, where ξ_j are independent random variables uniformly distributed in $[0, L]$, and $I_j = \{t : (j-1)T_w < t < jT_w\}$, that is, we consider a target hopping every T_w to a new random position between 0 and L. An outcome of our performance is shown in Figure 8.

Let us further investigate the tracking problem within interacting neuronal networks. The setup is similar to that in Figure 8A. An ensemble of 2000 LIF neurons is grouped into 10 columns. Neurons in different columns do not have interaction, but each 200 neurons in the same column interact with each other in an all-to-all connection with equations 3.1 and 3.2, and these 200 neurons share an identical tuning curve defined by equation 3.3. Figure 9A depicts the tuning curve and the estimate of $\lambda(x; x_i)$ by using the MLE method described above. The task of the tracking problem is to read out the position information $x(t)$. As shown in Figure 9B, the decoding is still accurate even though neurons in the network interact with each other.

4 Discussion

We have presented a study on how to perform MLE on spike waves. First, a rigorous algorithm of the MLE based on the ISI distribution is developed. The algorithm enabled us to address a few key issues in neuroscience. We have shown that the MLE can be successfully applied to read out either steady or dynamic inputs in single or pools of neurons. Even within short time windows, the decoded information is of high accuracy. We have also addressed that even for spiking neural networks with interactions, we can employ MLE to decode dynamic inputs by properly including the local inhibitory interactions in a microcolumn and the delay of synaptic currents.

We have included only a very brief account of our applications here and will publish more results (e.g. on tracking moving stimuli, decoding multistimuli, constructing IF-type visual cortex, and exploring the gamma

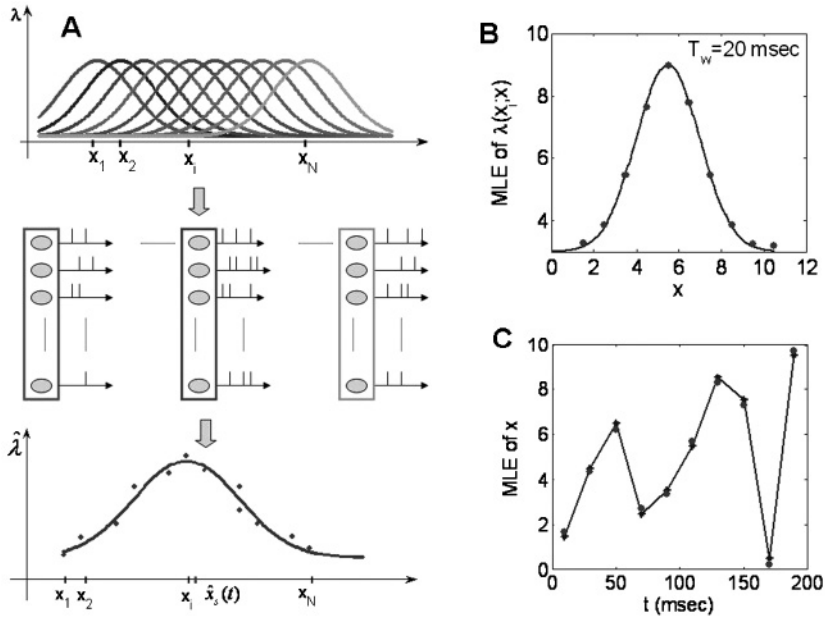

Figure 8: MLE in position tracking (the network is without interactions). (A) Setup of encoding and decoding. The place information $x(t)$ is fed to 1000 neurons organized in 10 columns with different preferred position x_i. For each column, spikes are collected in the window T_w, and the MLE is applied. The position is read out by first solving equation 3.3, obtaining the corresponding $\hat{x}$, and fitting a gaussian curve to all 10 data points $\hat{x}$. The maximum point of the fitted gaussian curve is the decoded position. (B) One example of $\hat{\lambda}$ versus columns. (C) An example of 10 decoded results of stimulus positions.

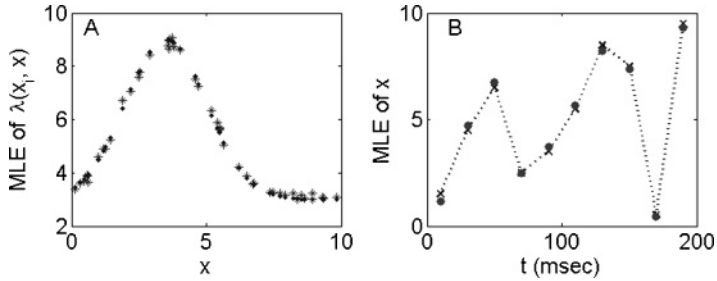

Figure 9: MLE in position tracking (the network is with interactions). (A) One example of the tuning curve (dots) and the estimate of $\lambda(x; x_i)$ (star points). (B) An example of decoding stimulus positions.

rhythm in signal decoding) elsewhere. Furthermore, our approach may help us to answer another long-standing problem: What is the ratio between inhibitory and excitatory inputs in a biological neuron? Although it has been found that the number of inhibitory neurons is smaller than the number of excitatory neurons in the cortex (Shadlen & Newsome, 1998; Leng et al., 2001), it is generally agreed that inhibitory neurons send stronger signals than excitatory neurons (Destexhe & Contreras, 2006). Therefore, the exact ratio between inhibitory and excitatory inputs remains elusive. With the MLE developed in this letter, we may be able to reliably estimate the ratio between inhibitory and excitatory inputs to a LIF neuron.

As a simplified phenomenological neuronal model, the LIF equation preserves spiking properties of a neuron, and the input information can be reliably read out, as we show here. However, the LIF model fails to capture many biophysical details. Some other models are more biophysically accurate but still mathematically simple, such as quadratic IF neurons (Feng & Brown, 2000a; Brunel & Latham, 2003), exponential IF neurons (Fourcaud-Trocme, Hansel, van Vreeswijk, & Brunel, 2003), and, more recently, adaptive exponential IF neurons (Brette & Gerstner, 2005). It is shown that adaptive exponential IF neurons give an effective description of neuron activities and can reliably predict the voltage trace of a naturalistic pyramidal neuron from a dynamic I-V curve (Badel et al., 2008). We realized that generalizing the MLE strategy developed for the LIF neurons to these nonlinear IF neurons needs more investigation, as it is not easy to derive exact expressions of the distributions of ISIs for these nonlinear IF neurons.

Appendix: Derivation of Equation 2.9

The probability density of the first hitting time of an Ornstein-Uhlenbeck (OU) process has been presented in the literature (Göing-Jaeschke & Yor, 2003; Alili et al., 2005). However, readers who are not familiar with stochastic process theory may not follow the mathematical proof there. In this appendix, we provide a derivation of equation 2.9 and explain the probability meaning of the expression.

A.1 Some Preliminary Results. We first introduce some stochastic processes related to equation 2.9.

Let $\mathbf{B} \stackrel{\Delta}{=} \{B_t\}_{t\geq 0}$ be a Brownian motion starting at $B_0 = x$ with its increment $B_{t+\Delta t} - B_t \sim N(0, \Delta t)$. If $x = 0$, then B is called a standard Brownian motion. Denote P_x^{BM} the corresponding probability law defined on the following sampling space,

$$\Omega = \{\omega : \omega(t) = X_t(\omega), t \geq 0\},$$

where $\{X_t\}_{t\geq 0}$ is the canonical process, with $\mathcal{F}_t = \sigma\{X_s, s \leq t\}$ being information before time t.

The OU process starting from $x \in R$ with parameter $\alpha \in R$ is the solution to the following stochastic differential equation:

$$dU_t = dB_t - \alpha U_t dt, \quad U_0 = x \in R. \tag{A.1}$$

Under the canonical measure P_x^{BM}, this process is no longer a Brownian motion. We hope to find a new law, denoted as $P_x^{OU(\alpha)}$, under which the process $W_t \triangleq B_t - \int_0^t U_s ds$, $t \geq 0$ is still a Brownian motion. Using the Girsanov theorem (the same idea was also employed in Feng & Brown (2000b)), we find that such a new law exists, and the density transformation from P_x^{BM} to $P_x^{OU(\alpha)}$ along the canonical path is given by

$$\frac{dP_x^{OU(\alpha)}}{dP_x^{BM}}(\omega) = \exp\left[-\frac{\alpha}{2}(B_t^2 - x^2 - t) - \frac{\alpha^2}{2}\int_0^t B_s^2 ds\right]. \tag{A.2}$$

Based on the Brownian motion, we can have another stochastic process, the so-called three-dimensional Bessel process $\{R(t)\}_{t\geq 0}$ starting at $R_0 = 0$, which is constructed from three independent standard Brownian motions $\{B_{i,t}\}_{t\geq 0}$, $i = 1, 2, 3$:

$$R_t \triangleq \sqrt{B_{1,t}^2 + B_{2,t}^2 + B_{3,t}^2}, t \geq 0. \tag{A.3}$$

R_t is actually the unique solution to the following stochastic differential equation,

$$dR_t = dB_t + \frac{n-1}{2R_t}dt, \quad R_0 = x \geq 0, \tag{A.4}$$

with $n = 3$, based on the following two facts:

1. The increment of a Brownian motion is of the order $\sqrt{dt}$, thus $dB_t^2 = 2B_t dB_t + dt$.
2. For two independent standard Brownian motions,

   $$B_{1,t}dB_{1,t} + B_{2,t}dB_{2,t} = \sqrt{B_{1,t}^2 + B_{2,t}^2}dB_t,$$

   where B_t is another standard Brownian motion.

A Brownian bridge $\{B_s^{x,y}\}_{0\leq s\leq t}$ from x to y of length t is a Brownian motion, given $(B_0 = x, B_t = y)$. Mathematically, it can be expressed as

$$B_s^{x,y} = x + B_s + \frac{s}{t}(y - x - B_t), 0 \leq s \leq t. \tag{A.5}$$

Starting from three independent Brownian bridge $\{B_{i,s}^{0,0}\}_{0\le s\le t}$, $i = 1, 2, 3$, the process

$$R_s^{x,y} \triangleq \sqrt{\left(x + \frac{s}{t}(y-x) + B_{1,s}^{0,0}\right)^2 + \left(B_{2,s}^{0,0}\right)^2 + \left(B_{3,s}^{0,0}\right)^2}, 0 \le s \le t \quad \text{(A.6)}$$

is the three-dimensional Bessel bridge from x to y of length t. Similar to the derivation of equation A.4 from A.3, $\{R_s^{x,y}\}_{0\le s\le t}$ can be characterized as the solution to the following stochastic process:

$$dr_s = \left(\frac{1}{r_s} + \frac{y - r_s}{t - s}\right) ds + dB_s, \quad 0 < s < t, \quad r_0 = x, r_t = y. \quad \text{(A.7)}$$

A.2 Distribution of the First Passage Time of the OU Process. Let $\{X_t\}_{t\ge 0}$ be a stochastic process and

$$\tau_a = \inf\{t \ge 0 : X_t = a\},$$

that is, τ_a is the first hitting time of the process $\{X_t\}_{t\ge 0}$ at a. Under the law P_x^{BM}, it is known that

$$P_x^{BM}(\tau_a \in dt) = \frac{a - x}{\sqrt{2\pi t^3}} \exp\left(-\frac{(a-x)^2}{2t}\right) dt, \quad for \quad a \ge x. \quad \text{(A.8)}$$

Our purpose is to seek the distribution of τ_a under law $P_x^{OU(\alpha)}$. According to equation A.2, we know that

$$\begin{aligned}
&dP_x^{OU(\alpha)}(\tau_a \in dt) \\
&= \int_{\{\tau_a \in dt\}} \exp\left[-\frac{\alpha}{2}(a^2 - x^2 - t) - \frac{\alpha^2}{2}\int_0^t B_s^2 ds\right] dP_x^{BM} \\
&= \exp\left[-\frac{\alpha}{2}(a^2 - x^2 - t)\right] \cdot E_x^{BM}\left[\exp\left(-\frac{\alpha^2}{2}\int_0^t B_s^2 ds\right) I_{\{\tau_a \in dt\}}\right] \\
&= \exp\left[-\frac{\alpha}{2}(a^2 - x^2 - t)\right] \cdot E_x^{BM}\left[\exp\left(-\frac{\alpha^2}{2}\int_0^t B_s^2 ds\right)\middle| \tau_a = t\right] \\
&\quad \cdot P_x^{BM}(\tau_a \in dt), \qquad \text{(A.9)}
\end{aligned}$$

where $E_x^{BM}[\cdot|\tau_a = t]$ is the expectation over Brownian motion $\{B_s\}_{s\ge 0}$ starting at x, given $\tau_a = t$. However, such a conditional expectation is not easy to find since the conditional event is a stopping time. We thus hope to find a new process, which can simplify the calculation along the path of this process.

A Brownian motion starting at x, given $\tau_a = t$, is a Brownian bridge from x to a of length t, given $\tau_a = t$. We write such a conditional Brownian bridge as

$$\left(B_s^{x,a}, 0 \le s \le \tau_a | \tau_a = t\right). \tag{A.10}$$

Let $Y_s^{x,a} = a + x - B_{t-s}^{x,a}, 0 \le s \le t$, also a bridge from x to a of length t. Since a Brownian bridge is gaussian, it is known that

$$\left(B_s^{x,a}, 0 \le s \le t\right) \stackrel{d}{=} \left(Y_s^{x,a}, 0 \le s \le t\right) \tag{A.11}$$

by checking the first and the second moments; here $\cdots \stackrel{d}{=} \cdots$ means "equal in a distribution sense."

Furthermore, given $\tau_a = t$, it is easily seen that

$$\sigma_a = \sup\{s : Y_s^{x,a} = a, 0 \le s \le t\} = \sup\{s : B_{\tau_a - s}^{x,a} = x, 0 \le s \le \tau_a\} = \tau_a. \tag{A.12}$$

This implies that if t is the first hitting time of the bridge $\{B_s^{x,a}\}_{0 \le s \le t}$ at a, then t is the last visiting time of the bridge $\{Y_s^{x,a}\}_{0 \le s \le t}$ at a. Equations A.11 and A.12 tell us that we can replace the Brownian bridge $(B_s^{x,a}, 0 \le s \le t)$, given $\tau_a = t$, by a new bridge $(Y_s^{x,a}, 0 \le s \le t)$ without conditions.

Then what is the law for this new bridge? Thanks to the Williams time-reversal theorem, the process $(Y_s^{x,a}, 0 \le s \le t)$ has the same distribution as a three-dimensional Bessel bridge $R_s^{x,a}$ from x to a of length t, which is the solution to equation A.7. As a rigorous proof for this result requires deep mathematical techniques related to stochastic processes, we will not repeat here but refer readers to corollary 4.4 in Revuz and Yor (1999).

We can now calculate $E_x^{BM}[\cdot | \tau_a = t]$. First, from an important fact that the process $(B_s^{x,a}, 0 \le s \le t)$ under the law P_x^{BM} is identical to $(a - B_s^{x,a}, s \ge 0)$ under the law P_{a-x}^{BM}, we conclude that for $a \ge x$,

$$\begin{aligned} &E_x^{BM}\left[\exp\left(-\frac{\alpha^2}{2}\int_0^t B_s^2 ds\right)\middle|\tau_a = t\right] \\ &\quad = E_{a-x}^{BM}\left[\exp\left(-\frac{\alpha^2}{2}\int_0^t (a - B_s)^2 ds\right)\middle|\tau_0 = t\right]. \end{aligned} \tag{A.13}$$

Second, based on the fact we discussed above that $(B_s^{a-x,0}, 0 \le s \le \tau_0 | \tau_0 = t)$ is actually a three-dimensional Bessel bridge from $a - x$ to 0 of

length t, we have

$$E_{a-x}^{BM}\left[\exp\left(-\frac{\alpha^2}{2}\int_0^t (a-B_s)^2 ds\right)\middle|\tau_0 = t\right] = E_{a-x}^{Bes}\left[\exp\left(-\frac{\alpha^2}{2}\int_0^t (R_s-a)^2 ds\right)\middle|R_t = 0\right]. \tag{A.14}$$

Third, based on

$$E_0^{Bes}[f(R_s)|R_t = a-x] = E[f(R_s)|R_0 = a-x,\, R_t = 0] = E[f(R_{t-s})|R_0 = 0,\, R_t = a-x],$$

we know that

$$\begin{aligned} &E_{a-x}^{Bes}\left[\exp\left(-\frac{\alpha^2}{2}\int_0^t (R_s-a)^2 ds\right)\middle|R_t = 0\right] \\ &= E_0^{Bes}\left[\exp\left(-\frac{\alpha^2}{2}\int_0^t (R_{t-s}-a)^2 ds\right)\middle|R_t = a-x\right] \\ &= E_0^{Bes}\left[\exp\left(-\frac{\alpha^2}{2}\int_0^t (R_s-a)^2 ds\right)\middle|R_t = a-x\right] \\ &= E_{0\to a-x}\left[\exp\left(-\frac{\alpha^2}{2}\int_0^t (r_s-a)^2 ds\right)\right], \end{aligned} \tag{A.15}$$

where $E_{0\to a-x}[\cdot]$ stands for the expectation of three-dimensional Bessel bridge $\{r_s\}_{s\le t}$ from 0 to $a-x$ over the interval $[0,t]$, which is the solution to equation A.7.

Therefore,

$$\begin{aligned} dP_x^{OU(\alpha)}(\tau_a \in dt) = &\exp\left[-\frac{\alpha}{2}(a^2-x^2-t)\right] \\ &\cdot E_{0\to a-x}\left[\exp\left(-\frac{\alpha^2}{2}\int_0^t (r_s-a)^2 ds\right)\right]\cdot P_x^{BM}(\tau_a \in dt), \end{aligned} \tag{A.16}$$

Set $P_x^{OU(\alpha)}(\tau_x \in dt) = p_{x\to a}^{(\alpha)}(t)dt$, and together with equation A.8, we have

$$\begin{aligned} p_{x\to a}^{(\alpha)}(t) = &\exp\left[-\frac{\alpha}{2}(a^2-x^2-t)\right] p_{0\to a-x}^{(0)}(t) \\ &\cdot E_{0\to a-x}\left[\exp\left(-\frac{\alpha^2}{2}\int_0^t (r_s-a)^2 ds\right)\right]. \end{aligned} \tag{A.17}$$

By replacing $x = -\frac{\mu\gamma}{\sqrt{\sigma}}$, $a = \frac{V_{th}-\mu\gamma}{\sqrt{\sigma}}$, $\alpha = \frac{1}{\gamma}$ and letting $v_s = \sqrt{\sigma} r_s$, we obtain the density equation 2.9 of ISIs of an LIF model, equation 2.2, and the corresponding three-dimensional Bessel bridge $\{v_s\}_{0\le s\le t}$ from 0 to V_{th}, which satisfies equation 2.11.

Acknowledgments

We are grateful to the referees for their useful comments, which improved this letter greatly. We benefited from discussions with M. P. Qian, E. Rossoni, and J. S. Xie. J.F. was partially supported by the CARMEN e-science project (www.carmen.org.uk) funded by the EPSRC (EP/E002331/1) and an EU grant BION. X.J. was partially supported by the National Natural Science Foundation of China (under grant nos. 10305007, 10771155) and a Foundation for the Author of National Excellent Doctoral Dissertation of PR China.

References

Alili, L., Patie, P., & Pedersen, J. L. (2005). Representations of the first hitting time density of an Ornstein-Uhlenbeck process. *Stochastic Models*, *21*, 967–980.

Badel, L., Lefort, S., Brette, R., Petersen, C. C. H., Gerstner, W., & Richardson, M. J. E. (2008). Dynamic I-V curves are reliable predictors of naturalistic pyramidal-neuron voltage traces. *J. Neurophysiol.*, *99*(2), 656–666.

Brunel, N., & Hakim, V. (2008). Sparsely synchronized neuronal oscillations. *Chaos*, *18*, 015113.

Brunel, N., & Latham, P. E. (2003). Firing rate of the noisy quadratic integrate-and-fire neuron. *Neural Computation*, *15*, 2281–2306.

Brette, R., & Gerstner, W. (2005). Adaptive exponential integrate-and-fire model as an effective description of neuronal activity. *J. Neurophysiol.*, *94*, 3637–3642.

Buzsáki. G. (2006). *Rhythms of the brain*. New York: Oxford University Presss.

Cateau, H., & Reyes, A. D. (2006). Relation between single neuron and population spiking statistics and effects on network activity. *Phys. Rev. Lett.*, *96*, 058101.

Deneve, S., Latham, P. E., & Pouget, A. (1999). Reading population codes: A neural implementation of ideal observers. *Nat. Neurosci.*, *2*, 740–745.

Destexhe. A., & Contreras, D. (2006). Neuronal computations with stochastic network states. *Science*, *314*, 85–90.

Ditlevsen, S., & Lansky, P. (2005). Estimation of the input parameters in the Ornstein-Uhlenbeck neuronal model. *Phys. Rev. E*, *71*, 011907.

Feng, J. F. (Ed.). (2003). *Computational neuroscience: A comprehensive approach*. London/Boca Raton, FL: Chapman and Hall/CRC, Press.

Feng, J. F., & Brown, D. (2000a). Integrate-and-fire models with nonlinear leakage. *Bull. Math. Biol.*, *62*(3), 467–481.

Feng, J., & Brown, D. (2000b). Impact of correlated inputs on the output of the integrate-and-fire models. *Neural Computation*, *12*, 671–692.

Feng, J. F., & Ding, M. (2004). Decoding spikes in a spiking neuronal network. *J. Phys. A: Math. and Gen.*, *37*, 5713–5727.

Fourcaud-Trocme, N., Hansel, D., van Vreeswijk, C., & Brunel, N. (2003). How spike generation mechanisms determine the neuronal response to fluctuating inputs. *J. Neurosci.*, *23*, 11628–11640.

Gardiner, C. W. (1985). *Handbook of stochastic methods: For physics, chemistry and the natural sciences*. Berlin: Springer.

Gerstner, W., & Kistler. W. (2002). *Spiking neuron models single neurons, populations, plasticity*. Cambridge: Cambridge University Press.

Göing-Jaeschke, A., & Yor, M. (2003). A clarification note about hitting times densities for Ornstein-Uhlenbeck processes. *Finance Stoch.*, *7*, 413–415.

Hung, C. P., Kreiman, G., Poggio, T., & DiCarlo, J. J. (2005). Fast readout of object identity from macaque inferior temporal. *Science*, *310*, 863–866.

Leng, G., Brown, C. H., Bull, P. M., Brown, D., Scullion, S., Currie, J., et al. (2001). Responses of magnocellular neurons to osmotic stimulation involves coactivation of excitatory and inhibitory input: An experimental and theoretical analysis. *J. Neurosci.*, *21*, 6967–6977.

Memmesheimer, R. M., & Timme, M. (2006). Designing the dynamics of spiking neural networks. *Phys. Rev. Lett.*, *97*, 188101.

Paninski, L., Pillow, J. W., & Simoncelli, E. P. (2004). Maximum likelihood estimation of a stochastic integrate-and-fire neural encoding model. *Neural Computation*, *16*, 2533–2561.

Revuz, D., & Yor, M. (1999). *Continuous martingales and Brownian motion* (3rd ed.). Berlin: Springer.

Rieke, F., Warland, D., & Steveninck, R. (1997). *Spikes: Exploring the neural code*. Cambridge, MA: MIT Press.

Risken, H., & Frank, T. (1984). *The Fokker-Planck equation: Methods of solutions and applications*. Berlin: Springer-Verlag.

Rossoni, E., & Feng, J. F. (2007). Decoding spike ensembles: Tracking a moving stimulus. *Biol. Cybern.*, *96*, 99–112.

Sanger, T. D. (2003). Neural population codes. *Curr. Opin. Neurobiol.*, *13*, 238–249.

Shadlen, M. N., & Newsome, W. T. (1994). Noise, neural codes and cortical organization. *Curr. Opin. Neurobiol.*, *4*(4), 569–579.

Shadlen, M. N., & Newsome, W. T. (1998). The variable discharge of cortical neurons: Implications for connectivity, computation, and information coding. *J. Neurosci.*, *18*, 3870–3896.

Stratonovich, R. L. (Ed.). (1967). *Topics in the theory of random noise: Mathematics and its applications*. Gordon and Breach Science Pub.

Truccolo, W., & Eden, U. (2005). A point process framework for relating neural spiking activity to spiking history, neural ensemble and covariate effects. *J. Neurophys.*, *93*, 1074–1089.

Thorpe, S., Fiz, D., & Marlot, C. (1996). Speed of processing in the human visual system. *Nature*, *381*, 520–522.

Tuckwell, H. C. (1988). Introduction to theoretical neurobiology. Cambridge: Cambridge University Press.

Received June 18, 2008; accepted March 9, 2009.